

NLO Calculation of Prompt Photon Production in DIS at HERA

P. Aurenche¹, Rahul Basu², M. Fontannaz³

¹ *LAPTH, Université de Savoie, CNRS,
BP 110, Chemin de Bellevue, 74941 Annecy-le-Vieux Cedex, France*

² *The Institute of Mathematical Sciences, Chennai 600 113, India*

³ *Laboratoire de Physique Théorique, UMR 8627 du CNRS,
Université Paris XI, Bâtiment 210, 91405 Orsay Cedex, France*

Abstract

We present a NLO calculation of prompt photon production in DIS. The calculation involves direct, fragmentation and resolved contributions. It is performed in the virtual-photon proton center-of-mass system. A comparison of the theoretical results with HERA data is carried out.

1 Introduction

The prompt photon production in DIS eP collisions is an interesting reaction involving, in the theoretical description provided by QCD, several perturbative and non perturbative quantities related to virtual and real photons. At first sight the subprocess associated with the prompt photon production appears particularly simple. It is the Compton effect of a virtual photon on a quark with a real photon and a quark in the final state: $\gamma^* + q \rightarrow \gamma + q$. The theoretical description of this process only requires the knowledge of the quark distributions in the proton and the calculation of Higher Order (HO) QCD corrections, the latter opening the way to a quantitative comparison with experimental data.

Actually, as always with photons, the situation is quite complex. We also have to consider the reaction in which the initial virtual photon fluctuates into a state made of collinear quarks and gluons described by the virtual photon structure function. In the final state also, a large- p_{\perp} quark can radiate a real collinear photon, a process which involves a perturbative part –the bremsstrahlung of the photon– and a non perturbative part, and which is described by the photon fragmentation function. Therefore the complete description of the prompt photon production requires the calculation of four classes of processes. Two classes involving the virtual photon structure function with the final photon either directly coupled to a quark of the hard subprocess (the resolved-direct process) or produced through the final fragmentation of a parton (the resolved-fragmented process). The two other classes involve the direct coupling of the virtual photon to a quark of the hard subprocess with a direct final photon (the direct-direct process) or with a photon fragment of a parton (the direct-fragmented process). All four processes corresponding to these four topologies having, as we shall see below, the same order of magnitude. Photons can also be emitted by the lepton line. We do not consider this contribution in this paper. It can be obtained, from ref. [1, 2].

On the experimental side, H1 and ZEUS [3, 4] have measured the prompt photon inclusive cross sections for which no QCD HO calculations exist. H1 also measured the production of a prompt photon associated with a jet. For this latter reaction a HO calculation does exist [2] which concerns the direct production. The fragmentation process is also taken into account and many observables are discussed in ref. [2]. It is the aim of this paper to present QCD HO calculations for the four processes of inclusive production of prompt photons in DIS eP collisions, and to compare the theoretical predictions with H1 and ZEUS data. We do not consider the production of a photon and a jet. But the approach of this paper is directly applicable to this latter case.

An important point in the definition of the prompt photon cross section is that of the reference frame in which the large- p_{\perp} photon is observed. There are two standards at HERA, the photon-proton (center of mass) CM system (hadronic system) and the laboratory frame. In the first one the observed large- p_{\perp} particle is produced, at lowest order, via $2 \rightarrow 2$ subprocesses. This frame has been used in almost all large- p_{\perp} reactions at HERA. We shall work in such a frame in the present paper. It is natural in photoproduction in which the almost real initial photon is collinear with the initial electron. For instance the photoproduction of prompt photons, which is the $Q^2 \rightarrow 0$ limit of the DIS reaction, has been studied in this frame [5, 6, 7]. A lower cut-off in p_{\perp} is necessary for perturbative QCD to be valid. The forward production of a π^0 , or a jet, in the DIS reaction has also been studied with this low-pt cut-off which picks $2 \rightarrow 2$ subprocesses (and their HO corrections) to produce large- p_{\perp} forward partons with the aim to test the importance of the BFKL dynamics [8, 9, 10, 11, 12, 13, 14, 15]. A detailed comparison with experimental results was performed and a good agreement of theoretical results with the data was found [11, 12, 15].

The situation is different in the laboratory in which a $2 \rightarrow 2$ subprocess is no more necessary to produce a large- p_{\perp} particle. The transverse momentum of the observed

photon may come from that of the virtual photon $q_{\perp} = \sqrt{Q^2(1-y)}$ (y being the inelasticity) through the basic DIS subprocess $\gamma^* + \text{quark} \rightarrow \text{quark}$, followed by the emission of the photon from the final quark. The authors of references [16] have proposed to use this frame as a way to attain the quark into photon fragmentation function, and have done a detailed study of this reaction at order $\mathcal{O}(\alpha^3)$.

Therefore the choice of a frame amounts to emphasize a given subprocess and the related non perturbative quantities. To be short one could say that the laboratory frame emphasizes the fragmentation part, whereas the $\gamma^* - P$ frame emphasizes the virtual photon structure function and the fragmentation part. Unfortunately only isolated photons have been observed at HERA, corresponding to a strong suppression of contributions involving fragmentation functions.

Of course it is not necessary to fix the transverse momentum and the rapidity of the observed photon in the $\gamma^* - P$ frame. This can be done in the laboratory. We only have to check that the subprocess in the $\gamma^* - P$ frame involves a large p_{\perp} scale. For instance H1, when observing forward (in the laboratory) and large- p_{\perp} (in the laboratory) π^0 , requires a cut on the transverse momentum of the π^0 in the hadronic frame [8]. We shall follow this procedure in this paper.

In the next section we give details on the HO calculations in the hadronic frame. In section 3 we present results for the inclusive cross section as a function of E_{\perp}^{γ} , y^{γ} and Q^2 . We discuss the effect of isolation (isolated prompt photons are measured by H1 and ZEUS). Then we examine, in section 4, the possibility to relate our $\gamma^* - P$ results with the H1 and ZEUS results obtained with no p_{\perp} cut in the hadronic frame. We will identify laboratory phase space regions in which this cut is not necessary to insure a large- p_{\perp} in the $\gamma^* - P$ frame. Section 5 is a conclusion.

2 Technical details

The programs containing a fragmentation function, which describe the resolved-fragmented and the direct-fragmented processes, can be immediately obtained from the programs of π^0 production in DIS eP reactions [13, 15]. The only change is that of the fragmentation functions; we now use the Bourhis-Fontannaz-Guillet (set II) [17] fragmentation functions.

The programs describing the direct-direct and resolved-direct processes can be obtained from the preceding ones by selecting the subprocesses with a final gluon and changing the charges and colour factors. Thus we obtain the cross sections corresponding to the emission of a photon.

In all these programs the HO corrections associated with a $2 \rightarrow 3$ subprocesses are calculated in dividing the phase space of the third final parton, which can be soft, in three parts: a small cylinder around the initial momenta (in the hadronic frame in which the virtual photon and the proton one collinear), a small cone around the two final hard partons, and the rest of the phase space. The cylinder allows us to treat the collinear and soft singularities associated with the initial partons. The cones allow us to calculate the collinear and soft singularities associated with the final partons. In the rest of the phase space the $2 \rightarrow 3$ cross sections have no singularities and the integration is performed by a Monte Carlo method [18].

This approach is described in details in references [19]. It is at the root of all the programs of the PHOX-FAMILY [20]. What is peculiar to DIS eP reactions is the presence of a virtual photon structure functions. Several problems are raised by these functions ; for instance the implementation of the $\overline{\text{MS}}$ factorization scheme, their NLO evolution, their parametrizations. A detailed discussion of all these points has been given in reference [14]. Here one can only keep in mind that the available NLO parametrization are given in the $\overline{\text{MS}}$ factorization scheme.

As only isolated photons are observed in the HERA experiments, we have im-

plemented an isolation criteria. We will use a cone criterion in the hadronic frame requiring no more than $\varepsilon E_{\perp}^{\gamma}$ hadronic transverse energy in a cone of radius R^{γ} surrounding the photon, with $\varepsilon = .1$ and $R^{\gamma} = 1$ (a value $\varepsilon = .111$ will be used when comparing theoretical results with H1 and ZEUS data¹).

The photon transverse energy can be fixed in the hadronic frame, in which we require a minimum value of the latter for a perturbative approach to be valid. This cut also eliminates contributions from the collinear subprocess $q + \gamma^* \rightarrow q$ followed by the bremsstrahlung of a final photon. The photon kinematics can also be fixed in the laboratory, as it is done by H1 and ZEUS. In this case, after a boost to the hadronic frame, the photon transverse energy may be very small. We suppress the contributions corresponding to this configuration by requiring again a minimum transverse energy in the hadronic frame. In the next section we present results obtained “in the laboratory frame” in order to be close to the kinematics used by the HERA experiments, but with a cut in the hadronic frame.

The calculations of the photon-jet cross sections could proceed in a similar way. We just have to introduce a jet algorithm in the routines calculating the $2 \rightarrow 3$ subprocesses, specifying how two final partons are combined to form a jet. The interest of the photon-jet cross sections is due to the simultaneous measurement of the photon p_{γ} and jet p_J four momenta, which allows us to define the invariant mass $m_{\gamma J}^2 = 2p_{\gamma} \cdot p_J$. Whatever the frame in which these momenta are measured, perturbative QCD calculations are valid if $m_{\gamma J}^2$ is large enough and we do not need any more a $p_{\perp\gamma}$ cut in the hadronic frame [2].

3 Cross sections in the hadronic frame

In this section we present the cross sections corresponding to the four topologies described in the introduction, and we consider non isolated and isolated photons.

¹The experimental cuts require that the photon carries at least 90% of the total energy of the jet of which it forms a part corresponding to $\varepsilon = .111$ with our conventions.

We adopt kinematical parameters close to those of the HERA experiments to make later comparisons with H1 and ZEUS easier. The beam energies of the proton and lepton are respectively 920 GeV and 27.6 GeV leading to $\sqrt{S_{ep}} = 318.7$ GeV. The inelasticity $y = \frac{q \cdot p}{\ell \cdot p}$ is taken in the range $.1 < y < .7$ and the photon virtuality Q^2 in the range $4 \text{ GeV}^2 < Q^2 < 100 \text{ GeV}^2$. (P , ℓ and q are the four momenta of the proton, the initial lepton and the virtual photon). The cross section involving the exchange of the Z -boson are neglected.

The rapidity of the photon in the laboratory frame is $1.8 > y_\gamma > -1.2$ and the transverse energy $10 \text{ GeV} > E_{\perp\gamma} > 3 \text{ GeV}$. In this section we do not consider the other cuts put by H1 and ZEUS on the scattering angle of the lepton, on the momentum of the outgoing lepton and on the invariant mass $(P + q - p_\gamma)^2 = W_x^2$ that we shall introduce in section 4 when comparing with data. Finally, in order to stay in a perturbative regime, we require the photon to have, in the hadronic frame, a minimum transverse momentum $p_{\perp\gamma}^* > 2.5 \text{ GeV}$.

We use the CTEQ6M distribution functions [23], the parton distributions in the virtual photon of ref. [14] and the BFG photon fragmentation functions (set II) [17]. We work with $N_f = 4$ flavors.

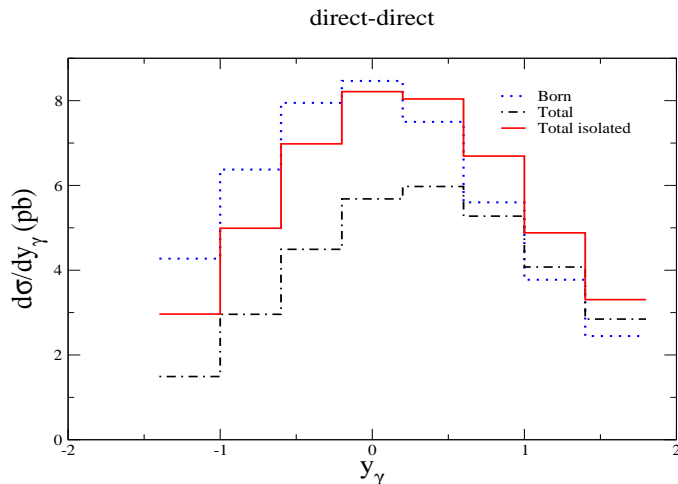


Figure 1: The direct-direct cross section $d\sigma/dy_\gamma$

Fig. 1 to Fig. 4 present the cross sections $d\sigma/dy_\gamma$ corresponding to the four topologies discussed in the introduction. We must keep in mind that these results are factorization scheme dependent. They depend on the initial factorization, final factorization and renormalization scales. Only the sum of the four partial cross sections has a physical meaning. The scales used in this section are $M = C\sqrt{Q^2 + (p_{\perp\gamma}^*)^2}$ for the proton factorization scale, $M_\gamma = \sqrt{Q^2 + (C_\gamma p_{\perp\gamma}^*)^2}$ for the virtual photon factorization scale, $M_F = C_F\sqrt{Q^2 + (p_{\perp\gamma}^*)^2}$ for the fragmentation factorization scale and $\mu = C_\mu\sqrt{Q^2 + (p_{\perp\gamma}^*)^2}$ for the renormalization scale, with $C = C_\gamma = C_F = C_\mu = 1$. All our calculations are performed in the $\overline{\text{MS}}$ factorization scheme. In particular the HO terms with a direct final photon are obtained from one-loop calculations from which final collinear singularities are subtracted with the $\overline{\text{MS}}$ convention.

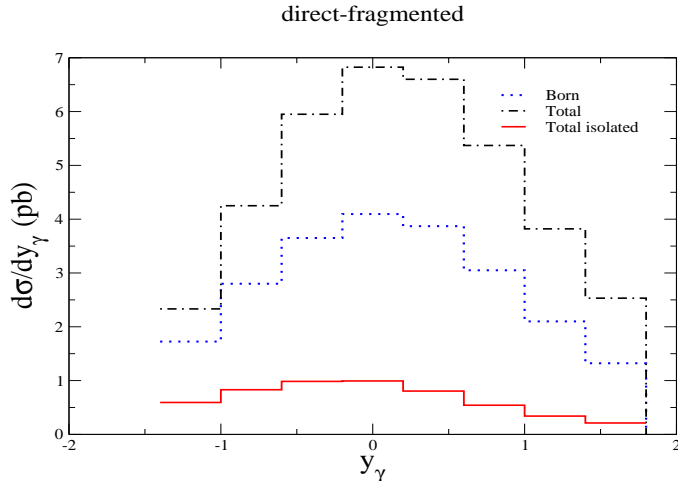


Figure 2: The direct-fragmented cross section $d\sigma/dy_\gamma$

Let us first consider the production of inclusive non isolated photons and let us start with the Born terms (Figs. 1-4). As expected the largest contribution comes from the direct-direct reaction. However the other reactions are not negligible. The direct-fragmented contribution is a factor 2 below the direct-direct one, and each of the resolved contributions another factor two below so that the direct-direct contribution represents only half of the full cross section.

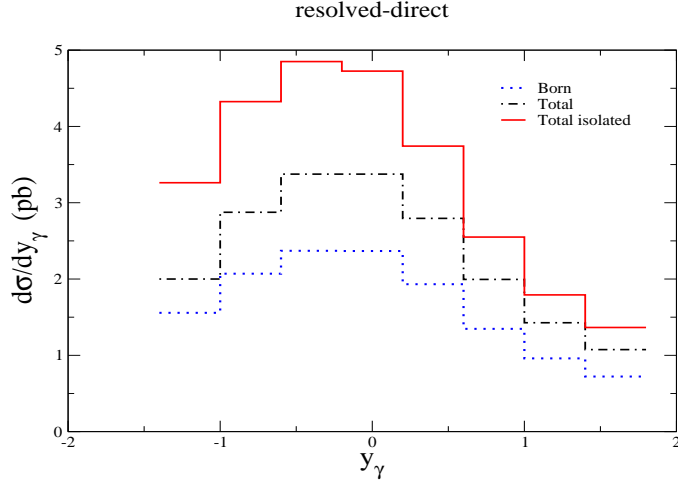


Figure 3: The resolved-direct cross section $d\sigma/dy_\gamma$

The HO corrections are important. We display in the figures the Total = Born + HO cross section for each class. The HO corrections almost double the Born terms for the components involving fragmentation. This is due to the large number of subprocesses participating in the cross sections. For the contributions with a final direct photon, the pattern is different. For instance in the direct-direct case the HO corrections are very negative for y_γ smaller than .5. This produces an important correction of the cross section especially in the negative y_γ range. The peculiarities of the direct-direct reaction is the presence of only one subprocess at the Born level, namely $\gamma^* + q \rightarrow \gamma + q$, and the presence of strong kinematical constraints (parton distributions in the photon and fragmentation functions replaced by delta-functions).

When the isolation is switched on, we obtain an interesting pattern of Born terms and HO corrections. As expected we have a strong decrease of the Born sections involving fragmentation functions of about a factor six, or even larger in the forward direction. Therefore these Born cross sections are almost negligible compared to the direct Born cross section on which the isolation has no effect. For the HO order corrections the decreases are less pronounced compared to the Born terms and they even increase in the cases of final direct photons; for instance by a

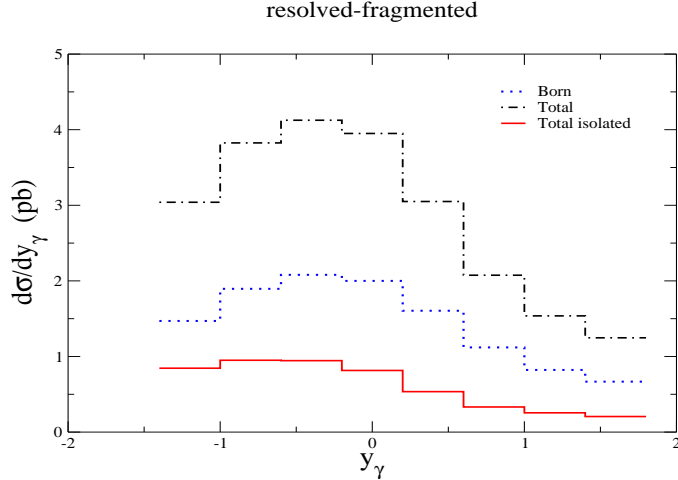


Figure 4: The resolved-fragmented cross section $d\sigma/dy_\gamma$

factor 2 for the resolved-direct case. This increase of the isolated total cross section, for the case where the photon is directly produced in the final state (Figs. 1 and 3), has already been observed and discussed in ref. [24] which studies the prompt photon production in hadron-hadron collisions. It is due to the fact that some HO final collinear contributions are subtracted from the HO direct cross section to build the fragmentation functions. The remaining collinear terms are negative and the subtracted HO direct contribution increases when these negative terms are cut by the isolation. Of course this effect is factorization scheme dependent and demonstrates once more that only the sum of the cross sections has a physical meaning (the total cross section must decrease when the isolation is switched on).

In conclusion, we observe that the resolved-direct isolated cross section is larger than the non isolated one (Fig. 3). This is also true for the direct-direct cross section with a very different behavior in rapidity (Fig. 1). The isolated resolved-fragmented and the direct-fragmented cross sections are small compared to the isolated resolved-direct and direct-direct contributions, but not totally negligible.

In Figs. 5 and 6 we finally show the contributions of the resolved and the direct

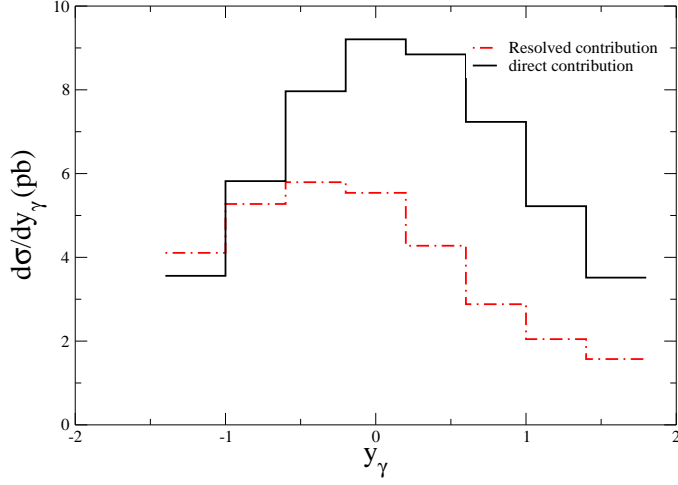


Figure 5: Resolved and direct isolated cross sections $d\sigma/dy_\gamma$.

processes for the cross section $d\sigma/dy_\gamma$ and $d\sigma/dE_{\perp\gamma}$ (isolated case). These figures illustrate the non negligible contributions of the resolved components specially for negative values of the photon rapidity.

4 Comparison with experimental results

Unlike what was done until now for the production of large p_\perp hadrons or jets, the H1 and ZEUS experiments do not put, in the case of prompt photons, kinematical cuts in the hadronic system and it is easy to check that their laboratory cuts do not protect the hadronic system $p_{\perp\gamma}^*$ against small numerical values. Thus the possibility of performing a perturbative calculation is not ensured. The values of Q^2 and y being fixed by the observation of the outgoing lepton, we have to calculate the expression

$$\int dQ^2 dy \int \frac{dx}{x} G(x) \frac{\ell^{\mu\nu} t_{\mu\nu}}{Q^4} \delta^{(4)}(p + q - p_4 - p_3) d\vec{p}_{\perp 4} dy_4 d\vec{p}_{\perp 3} dy_3, \quad (4.1)$$

the definition of the momenta being given in Fig. 7a corresponding to the laboratory frame.

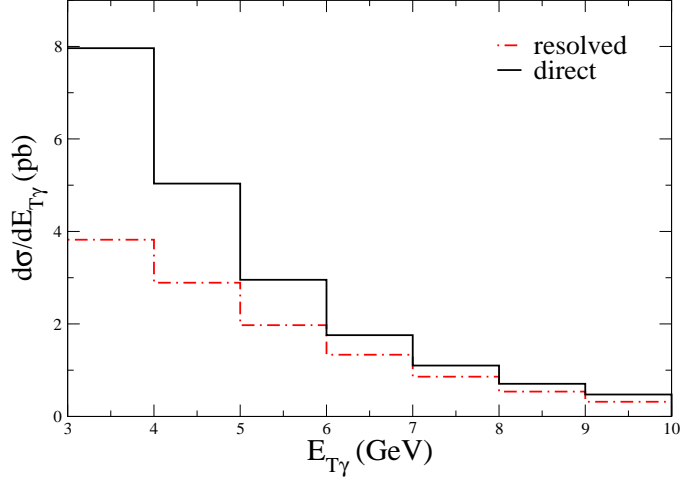


Figure 6: Resolved and direct isolated cross sections $d\sigma/dE_{\perp\gamma}$.

The delta-function can be written in terms of the light cone variables, transverse momenta and rapidities.

$$\begin{aligned}
& 2\delta^{(2)}(\vec{q}_{\perp} - \vec{p}_{4\perp} - \vec{p}_{3\perp}) \delta\left(xP^{(+)} - \frac{Q^2}{\ell^{(-)}} - p_{\perp 4} e^{y_4} - p_{\perp 3} e^{y_3}\right) \delta\left(y\ell^{(-)} - p_{\perp 4} e^{-y_4} - p_{\perp 3} e^{-y_3}\right) \\
&= \frac{2}{P^{(+)}\ell^{(-)}} \delta^{(2)}(\vec{q}_{\perp} - \vec{p}_{4\perp} - \vec{p}_{3\perp}) \delta\left(x - \frac{Q^2 y}{2P \cdot q} - \frac{p_{\perp 4} e^{y_4} + P_{\perp 3} e^{y_3}}{p^{(+)}}\right) \\
& \delta\left(y - \frac{p_{\perp 4} e^{-y_4} + p_{\perp 3} e^{-y_3}}{\ell^{(-)}}\right) \tag{4.2}
\end{aligned}$$

with

$$P^{(+)} = P_0 + P_z = 2P_z$$

$$\ell^{(-)} = \ell_0 - \ell_z = 2E$$

and $p^{(+)} = xP^{(+)}$.

From (4.2) we obtain the following constraints

$$\begin{aligned}
e^{y_4} &= \frac{p_{\perp 4}}{y\ell^{(-)} - p_{\perp 3} e^{-y_3}} \quad \text{and} \\
\vec{p}_{\perp 4} &= \vec{q}_{\perp} - \vec{p}_{\perp 3} . \tag{4.3}
\end{aligned}$$

We see that we can ensure a minimum value of $\hat{s} = \mathcal{O}(p_{\perp 3} p_{\perp 4})$, the subprocess center-of-mass energy squared, with the requirement $\sqrt{Q^2(1-y)} = |\vec{q}_{\perp}| < |\vec{p}_{\perp 4}|$.

To discuss the constraints on y_4 let us consider the extreme case where \vec{p}_3 is parallel to \vec{p}_4 ($\hat{s} = 0$). With the definition $q_{\perp} = p_{\perp 3} + p_{\perp 4}$ and with $y_3 = y_4$ we get from the constraints (4.2)

$$\begin{aligned} x = x_{B_j} &= \frac{Q^2}{y S_{ep}} \\ e^{y_4} &= \frac{\sqrt{Q^2(1-y)}}{2y\ell^0}. \end{aligned} \quad (4.4)$$

The first result is the standard constraint associated with the $q + \gamma^* \rightarrow q$ subprocess; the second result shows that y_4 cannot be large if Q^2 is small and y bounded from below. This can be rewritten as $q_{\perp} = e^{y_4} 2\ell^0 y$. With the H1 cut $y_{min} = .05$ we obtain $p_{\perp min} = 2.76 e^{y_4}$, which shows that the collinear configuration ($\hat{s} = 0$) does not contribute to the cross section in the small p_{\perp} and large y_4 domain.

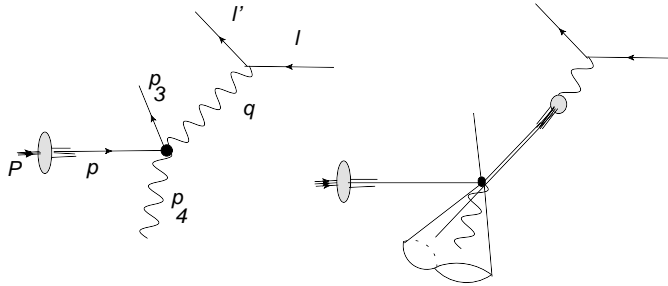


Figure 7: a) direct-direct kinematics in the LAB frame. b) idem for the resolved-direct subprocess.

4.1 Comparison with H1 data

To determine the exact phase space domain in which our calculation is valid, we explore, for large value of y_4 or for small values of Q^2 , the sensitivity of the cross section to $p_{\perp \gamma^*}$ - cuts. In this study we switch to the exact H1 cuts which include the conditions $E'_e > 10$ GeV, $153^\circ < \theta_e < 177^\circ$ and $W_x > 50$ GeV. Now the values of the

inelasticity y are bounded below by $.05 < y$, and we have $4 < Q^2 < 150 \text{ GeV}^2$. We also implement the isolation criterion in the laboratory frame by requiring a limited hadronic energy E_{\perp}^h in a cone of radius R^{γ} around the photon. This isolation is different from that defined in the hadronic frame since parton 3 (fig. 7) can now be inside the isolation cone because of the transverse boost provided by the virtual photon. We use the isolation parameters $\varepsilon = .111$ and $R^{\gamma} = 1$. We perform our exploration of the “safe” domains by studying the direct-direct cross section. A typical result that we obtain for the small Q^2 domain $4 \leq Q^2 \lesssim 10 \text{ GeV}^2$ is given in table 1. All other H1 parameters and cuts being as given above.

$p_{\perp\gamma}^*$ -cut	Born	NLO
2.5 GeV	6.60	$7.14 \pm .05$
1.5 GeV	7.50	$7.64 \pm .05$
.5 GeV	7.60	$7.62 \pm .05$

Table 1: Integrated direct-direct cross section in the range $4 \leq Q^2 \leq 10 \text{ GeV}^2$ in picobarns.

We notice, as expected, a very small dependence on $p_{\perp\gamma}^*$ -cut. Exploration of the range $10 \leq Q^2 \leq 20 \text{ GeV}^2$ leads to a much pronounced dependence on $p_{\perp\gamma}^*$ -cut, the cross section (Born term) varying from 4.82 to 7.2 pb. Interesting results are also given by H1 for the range $4 \leq Q^2 \leq 40 \text{ GeV}^2$, the laboratory transverse momentum $q_{\perp} = \sqrt{Q^2(1-y)} \leq$ being not too large compared to $E_{\perp\gamma}$. We explore for this Q^2 range the large y_{γ} range $1.4 \leq y_{\gamma} \leq 1.8$ and find for the cross section a smaller variation than the one shown in table 1.

To conclude we find small variations of the cross section with $p_{\perp\gamma}^*$ -cut in the small Q^2 -range or in the large y_{γ} range. This incites us to compare our predictions with H1 data in the above domains. The H1 collaboration provides us with data in

the domain $A : 4 < Q^2 < 10 \text{ GeV}^2, 3 < E_{\perp\gamma} < 10 \text{ GeV}, -1.2 < y_\gamma < 1.8$, in the domain $B : 4 < Q^2 < 40 \text{ GeV}^2, 6 < E_{\perp\gamma} < 10 \text{ GeV}, -1.2 < y_\gamma < 1.8$, and in the domain $C : 4 < Q^2 < 40 \text{ GeV}^2, 3 < E_{\perp\gamma} < 10 \text{ GeV}, 1.4 < y_\gamma < 1.8$. In these three domains the variations with $p_{\perp\gamma}^*$ -cut of the cross section is small, especially domains B and C . In the first domain the stability of the resolved-direct (rd) cross section is not as good as than that of the direct-direct (dd) contribution of table 1. It varies for 4.45 to 5.91 for $p_{\perp\gamma}^*$ -cut ranging from 2.5 GeV to .5 GeV.

Our predictions are compared with data in table 3 and details of the contributions are given in table 2. In these three domains we set $p_{\perp\gamma}^*$ -cut = 1.0 GeV.

Domain	dd contribution		rd contribution		df contribution	
	Born	NLO	Born	NLO	Born	NLO
A	1.26	1.27	.59	1.18	.0785	.192 pb/GeV ²
B	.74	.67	.32	.56	.0475	.098 pb/GeV
C	3.72	4.66	1.02	1.88	.153	.370 pb

Table 2: Details of the dd , rd and df contributions.

Domain	Data	f_{had}	dd + rd + df NLO
A	$2.48 \pm .21$ ^{+.34} _{-.41}	.87	2.30 pb/GeV ²
B	$1.78 \pm .25$ ^{+.46} _{-.60}	.97	1.29 pb/GeV
C	4.38 ± 1.26 ^{+1.04} _{-1.75}	.77	5.32 pb

Table 3: Comparison between data and theory.

In the three domains² we find a good agreement between theory and experiment. Note that the last column of table 3 has been obtained by multiplying the predictions of table 2 by the hadronic correction factors f_{had} given by H1 [3]. The small resolved-fragmented contribution has not been taken into account; we estimate this contribution to be approximatively equal to 6 % of the total cross sections. Note also that the contributions due to the emission of photons by the lepton line is not taken into account. The H1 collaboration has estimated this contribution [3]. It is almost negligible (~ 5 %) in domain A , it represents about 13 % of the theoretical cross section (table 3) in domain B , and is totally negligible in domain C .

4.2 Comparison with ZEUS data

The ZEUS collaboration measured the isolated photon cross section at the energy $\sqrt{S_{ep}} = 318$ GeV using the following cuts: $E'_e > 10$ GeV, $139.8^\circ < \theta_e < 171.9^\circ$ and $W_x > 5$ GeV. The kinematical domain covered by the experiment is: $10 < Q^2 < 350$ GeV², $4 < E_{\perp\gamma} < 15$ GeV and $-0.7 < y_\gamma < 0.9$. The data are quoted in various bins for each of these three variables with the other two variables integrated over the whole indicated range. From our previous discussion on H1 data it appeared that stability of our predictions under the $p_{\perp\gamma}^*$ cut-off could be achieved for low $Q^2 < 10$ GeV², or large photon rapidity $y_\gamma > 1.4$ with moderate Q^2 values, however none of these domains can be extracted from the published ZEUS data. Restricting to large $E_{\perp\gamma}$ values, *e.g.* $E_{\perp\gamma} > 10$ GeV, we have tested that it is impossible to obtain stability in the full Q^2 range of ZEUS. A relative stability of our predictions is achieved, however, when one restricts the Q^2 range between 10 and 20 GeV² integrating over the whole range for the other variables: we find a cross section (with only the d-d and d-f contributions) decreasing from .164 down

²The data in domains B and C have been obtained by subtraction between the $4 < Q^2 < 150$ and $40 < Q^2 \leq 150$. Statistical errors are added in quadrature and we keep the largest systematic errors.

to $.152 \text{ pb/GeV}^2$, when decreasing the cut-off from 2.5 to 1. GeV (the d-d HO are not stable). Multiplying the result by a factor 2 to roughly take into account the resolved contribution, we obtain a cross section of $.37 \text{ pb/GeV}^2$ (including a contribution of $.045 \text{ pb/GeV}^2$ from the lepton line) compatible with the value of $.414 \pm .035$ (stat.) pb/GeV^2 given by ZEUS.

5 Conclusions

A complete calculation of the isolated photon cross section in deep inelastic scattering has been presented at the next to leading logarithmic order in QCD. Isolation can be imposed in the hadronic center of mass frame or in the laboratory frame. The calculation includes four classes of processes depending on whether the photon is coupled directly to the hard process or through structure or fragmentation functions and it is valid if the momentum of the photon in the hadronic center of mass frame is large enough to prevent the $2 \rightarrow 1$ process, $q \rightarrow q + \gamma$, to occur in a collinear configuration. Unfortunately the H1 and ZEUS collaborations for their isolated prompt photon studies do not impose a transverse momentum cut-off in the hadronic center of mass frame but in the laboratory frame. This is unlike what was done for their studies on particle or jet production. The comparison between our calculation and the data can be performed only in a very restricted domain of the data: small Q^2 and/or large photon rapidity. It would be interesting if data could be available with a transverse momentum cut in the hadronic frame: a comparison with large transverse momentum π^0 production, will then be possible and it is an exercise always worth making as is done in hadronic colliders. The basic mechanisms of photon and π^0 production are different and so are the higher order corrections: a detailed comparison of theory with data in the case of photon production with many kinematical variables at hand ($Q^2, E_{\perp\gamma}, y_{\gamma}, x_{Bj}$) will be very constraining, as it was for π^0 production.

References

- [1] RAPGAP, H. Jung, Comput. Phys. Commun. **86** (1995) 147.
- [2] A. Gehrmann-De Ridder, G. Kramer and H. Spiesberger, Nucl. Phys. **B578** (2000) 326.
- [3] H1 collaboration, F.D. Aaron et al., Eur. Phys. J. **C54** (2008) 371.
- [4] ZEUS collaboration, S. Chekanov et al., Phys. Lett. **B687** (2010) 16.
- [5] ZEUS collaboration, S. Chekanov et al., Eur. Phys. J. **C49** (2007) 511.
- [6] H1 collaboration, F.D. Aaron et al., Eur. Phys. J. **C66** (2010) 17.
- [7] M. Fontannaz, J. Ph. Guillet and G. Heinrich, Eur. Phys. J. **C21** (2001) 303.
M. Fontannaz and G. Heinrich, Eur. Phys. J. **C34** (2004) 191.
- [8] H1 collaboration, A. Aktas et al., Eur. Phys. J. **C36** (2004) 191.
H1 collaboration, A. Aktas et al., Eur. Phys. J. **C46** (2006) 27.
- [9] ZEUS collaboration, S. Chekanov et al., Eur. Phys. J. **C52** (2007) 515.
- [10] G. Kramer and B. Pötter, Phys. Lett. **B453** (1999) 295.
- [11] A. Daleo, C.A. Garcia Canal and R. Sassot, Eur. Phys. J. **C33** (2004) 404.
A. Daleo, D. de Florian and R. Sassot, Phys. Rev. **D71** (2005) 034013.
- [12] B.A. Kniehl, G. Kramer and M. Maniatis, Nucl. Phys. **B711** (2005) 345, E :
B720 (2005) 231.
- [13] P. Aurenche, R. Basu, M. Fontannaz and R.M. Godbole, Eur. Phys. J. **C34** (2004) 277.
- [14] M. Fontannaz, Eur. Phys. J. **C38** (2004) 297.

- [15] P. Aurenche, R. Basu, M. Fontannaz and R.M. Godbole, Eur. Phys. J. **C42** (2005) 43.
- [16] A. Gehrmann-De Ridder, T. Gehrmann and E. Poulsen, Eur. Phys. J. **C47** (2006) 395.
- [17] L. Bourhis, M. Fontannaz, J. Ph. Guillet, Eur. Phys. J. **C2** (1998) 529.
- [18] S. Kawabata, BASES integration package, Comp.Phys.Comm. 88(1995) 309
- [19] T. Binoth, J. Ph. Guillet, E. Pilon, M. Werlen, Eur. Phys. J. **C16** (2000) 311.
P. Aurenche, L. Bourhis, M. Fontannaz, J. Ph. Guillet, Eur. Phys. J. **C17** (2000) 413.
- [20] P. Aurenche, T. Binoth, M. Fontannaz, J. Ph Guillet, G. Heinrich, E. Pilon, M. Werlen, <http://lappweb.in2p3.fr/PHOX-FAMILY/main.html>.
- [21] S.D. Ellis and D.E. Soper, Phys. Rev. **D48** (1993) 3160.
- [22] G. Salam, Towards Jetography, arXiv:0906.1833 [hep-ph].
- [23] J. Pumplin, D.R. Stump, J. Huston, H.L. Lai, P. Nadolsky and W.K. Tung, JHEP **0207** (2002) 012.
- [24] S. Catani, M. Fontannaz, J. Ph. Guillet, E. Pilon, JHEP 0205 (2002) 028